Shaping of sessile magnetic drops due to electromagnetic stress

Shaping of sessile magnetic drops due to electromagnetic stress

Jennifer Dodoo, and Adam A. Stokes*
School of Engineering, Institute for Micro and Nano Systems, The University of Edinburgh, Edinburgh, EH9 3LJ

Glen McHale
Smart Materials & Surfaces Laboratory, Faculty of Engineering and Environment, Northumbria University, Newcastle upon Tyne, NE1 8ST

(Dated: August 15, 2019)

While electric fields have been widely studied for drop shaping and digital microfluidics, a unified electromagnetic approach inclusive of magnetic fields is by far less known. Here using the electromagnetic stress tensor, we derive the stress acting on a droplet and test the results experimentally by measuring the shape of a paramagnetic drop in a magnetic field. We show through a simple transformation that our model can be applied to shaping of droplets by electric fields, thus giving a holistic description of the electromagnetic stresses acting on drops. This provides a blueprint for controlled shaping of sessile magnetic drops and has application to magnetic technologies in displays, liquid lenses, and chemical mixing of drops in microfluidics.

Controlled shaping of small volumes of fluids (or drops) is a key ingredient for liquid lenses to set optical properties [1], and for digital microfluidics (DMF) [2–4], where drops are, for example, manipulated for chemical mixing [5]. Drops can be shaped through the application of electromagnetic fields which exert a force on ions, and electric and magnetic dipoles in the drop. These forces can be calculated using the electromagnetic stress tensor, which is a powerful tool derived from first principles of electromagnetism and thermodynamics [6], and generally depends on: the thermodynamic potential of the system; the electric permittivity; the magnetic susceptibility; and the electromagnetic field applied. The electromagnetic stress tensor in vacuum (Maxwell stress tensor) has succesfully been applied to electrowetting - a technique where surface energies of the substrate are electrostatically modified - and dielectrophoresis, where a non-uniform electric field is applied to electric dipoles [7–10]. In contrast to the Maxwell stress tensor, which contains no information about the thermodyamic potential of the system, the full electromagnetic stress tensor, which contains this information, is generally not explicitly applied and evaluated, leading to common misconceptions about the model's range of validity [6].

Electrowetting is the most commonly used technique in DMF, but requires contact between the electrodes and the drop [2]. More recently, liquid dielectrophoresis, a contact-free bulk effect, is explored for DMF and liquid optics [10, 11] and has been successfully implemented for DMF manipulations [12]. Magnetic actuation techniques stand in contrast to electric actuation techniques, which dominate the DMF literature [4]. They open a range of new applications: magnetic fields are not as easily shielded as electric fields, making them suitable for applications in vivo or in environments that are sensitive to electric fields.

Magnetic techniques require the presence of magnetic dipoles and include: liquid marbles created using magnetic particles to enclose the drop; the actuation of fluids through the deformation of magnetic substrates; or the actuation of magnetic particle suspensions, such as ferrofluids [13, 14]. Ferrofluids are commonly used, because their high magnetic susceptibility values ($\chi > 10,000$) mean they can be actuated at low field strength. The application of magnetic fields pulls suspended particles into high-density regions, introducing an asymmetry in concentration that needs to be addressed in any formal treatment of ferrofluids. Paramagnetic salt solutions have a much smaller χ ($<< 1$) than ferrofluids, adding the benefit of uniformly distributed magnetic particles, even on application of a magnetic field. This alternative 'particle-free' actuation method has been demonstrated on superhydrophobic surfaces and a strong correlation between χ and ease of actuation has been shown [15, 16].

Here, we explicitly apply the electromagnetic stress tensor to a sessile drop in a magnetic field and derive a relationship for the change in drop shape as a function of applied magnetic field. We validate this relationship experimentally by measuring the change in shape of a paramagnetic sessile drop on a hydrophobic substrate in a homogeneous magnetic field. Our results highlight the fundamental symmetry in the shaping of drops with electric and magnetic fields.

The equilibrium shape of a sessile drop is determined by the stresses acting on it; these may include but are not limited to interfacial, gravitational and electromagnetic stress. To derive an expression for the shape of a sessile drop, we follow an analogous method to the one presented by Stierstadt and Liu [6] and use their definition of the full electromagnetic stress tensor which is universally valid for time-independent (quasi-static) non-dissipative processes:

$$\sigma_{ik} = (\mathrm{U} - \mathrm{TS} - \xi_\alpha \rho_\alpha - \mathbf{E}\cdot\mathbf{D} - \mathbf{H}\cdot\mathbf{B})\delta_{ik} + \mathrm{E_i D_k} + \mathrm{H_i B_k} \quad (1)$$

where i is the direction of force and k is the direction normal to the surface to which the force is applied, U is the total energy density of matter and field ($\mathrm{Jm^{-3}}$), T is temperature (K), S is the entropy of matter and field ($\mathrm{Jm^{-3}K^{-1}}$), ξ_α is the mass density of the chemical potential ($\mathrm{J\ kg^{-1}}$) of the material component α, ρ_α is the partial density of the material component α (the total density is $\rho^{\mathrm{tot}} = \Sigma_\alpha \rho_\alpha$), $\mathbf{E}$ is the electric field strength, $\mathbf{D}$ is the electrical displacement, $\mathbf{H}$ is the auxiliary field, $\mathbf{B}$ is the magnetic flux density, and δ_{ik} is the Kronecker-Delta function.

In this work, we assume that there are no electric fields acting on the drop ($\mathbf{D}$=$\mathbf{E}$=0) and that the magnetic susceptibility is independent of the applied magnetic field strength ($\mathbf{B} = \mu\mathbf{H} = \mu_0(1+\chi)\mathbf{H}$ and $\mathbf{M} = \chi\mathbf{H}$). We limit this analysis to a closed thermodynamic system at constant temperature and volume, which is suitably described by the Helmholtz potential ($\mathrm{U} = \mathrm{a^t} + \mathrm{TS}$). The thermodynamic potential can be separated into field-independent ($\mathrm{a_0}$) and field-dependent ($\mathrm{a_{em}}$) terms: $\mathrm{a^t} = \mathrm{a_0} + \mathrm{a_{em}}$, with $\mathrm{a_{em}} = \int \mathbf{H}\cdot\mathbf{dB}$.

The definition of the mass density of the chemical potential is: $\xi_\alpha = \delta \mathrm{a^t}/\delta\rho_\alpha$ [6]. In equilibrium, the stresses on the boundary of the two substances from inside and outside must be equal. The vapour phase is air, which we approximate as vacuum in its magnetic properties ($\mu = \mu_0$) as well as in its chemical potential ($\xi_\alpha \rho_\alpha = 0$). We impose the standard boundary conditions for Maxwell's equations as formulated by Stierstadt and Liu [6]: (1) the difference in the magnetic field component tangential to the surface must vanish ($\Delta \mathrm{B_t} = \Delta \mathrm{H_t} = 0$); (2) the stress components normal to the interface, σ_{nn}, must be continuous, while tangential components cancel. The electromagnetic stress difference across the air-liquid boundary then becomes:

$$\Delta\sigma_{nn}^{EM} = a_0^l - a_0^v - \xi_0\rho_\alpha - \frac{\mu_0}{2}H^2\left(\chi + \rho_\alpha\frac{\delta\chi}{\delta\rho_\alpha}\right) + \mu_0\chi H_n^2 \quad (2)$$

The magnetic flux density is the vector sum of its normal and tangential components with respect to the surface over which $\Delta\sigma_{\mathrm{nn}}^{\mathrm{EM}}$ is resolved, $\mathrm{H^2} = \mathrm{H_n^2} + \mathrm{H_t^2}$. We calculate the chemical potential using the Clausius-Mossotti approach: $\rho(\delta\chi/\delta\rho) = \chi(1+\chi/3) \approx \chi$ for one-component fluids with $\chi << 1$.

$$\Delta\sigma_{nn}^{EM} = a_0^l - a_0^v - \xi_0\rho + \frac{\chi}{\mu_0}\left(B_n^2 - B^2\right) \quad (3)$$

where B is the magnetic flux density in air (T). In addition to the electromagnetic stress difference, the shape of the drop is also determined by the stress differences due to gravity and surface tension:

$$\Delta\sigma_{nn}^{surf} = \gamma(R_1^{-1} + R_2^{-1}) \quad (4)$$

$$\Delta\sigma_{nn}^{grav} = g\Delta\rho z \quad (5)$$

where γ is the surface tension ($\mathrm{Nm^{-1}}$), $\mathrm{R_1}$ and $\mathrm{R_2}$ are the principle radii of curvature of the drop outline (m), g is the gravitational acceleration ($\mathrm{ms^{-2}}$), ρ is the mass density ($\mathrm{kgm^{-3}}$), and z is the vertical distance to the apex point (m), as indicated by Fig. 1 [6, 17]. The principle radii of curvature of an axisymmetric drop can be expressed as:

$$(R_1^{-1} + R_2^{-1}) = \frac{r''}{(1+r'^2)^{3/2}} - \frac{1}{r(1+r'^2)^{1/2}} \quad (6)$$

where r(z) is the drop outline, originating from the apex point, r' and r'' are the first and second derivatives of r with respect to z, and r(z) and r′ vanish at the apex point where z=0 [18]. In equilibrium, the stresses on the drop must sum up to zero.

$$0 = \Delta\sigma_{nn}^{surf} + \Delta\sigma_{nn}^{grav} + \Delta\sigma_{nn}^{EM} \quad (7)$$

Eq. (7) is an augmented Young-Laplace equation, which describes the hydrostatic and magnetic stresses on a sessile magnetic drop in air due to a magnetic field. Note that the definition of the magnetic stress in Eq. (2) holds for ferrofluids and para- and diamagnetic salt solutions and is valid in any time-independent (static) magnetic field. For axisymmetric drops, the radius of curvature at the apex point, b, depends on the difference of the energy densities of the Helmholtz potential of the liquid and vapour phase, $2\gamma\mathrm{b^{-1}} = \mathrm{a_0^l} - \mathrm{a_0^v}$ [6]. In the absence of magnetic fields, $\mathbf{B}$=$\mathbf{H}$=0, the stress balance of the drop simplifies to $0 = (\mathrm{R_1^{-1}} + \mathrm{R_2^{-1}}) + 2\mathrm{b^{-1}} + (\mathrm{g}\Delta\rho\gamma^{-1})\mathrm{z}$, which is the well-known Young-Laplace equation [17–19]. Eq. (2) can be applied to static electric fields through a simple transformation of $\mathbf{H} \to \mathbf{E}$, $\mu_0 \to \epsilon_0$ and $\chi \to \chi_e$ (electric susceptibility), due to the symmetric and additive nature of the electromagnetic stress tensor with regards to electric and magnetic contributions [6]. Using this transformation on Eq. (2) we obtain the electric stress difference across the air-liquid boundary: $\Delta\sigma_{\mathrm{nn}}^{\mathrm{EM}} = 2\gamma\mathrm{b^{-1}} - \xi_0\rho_\alpha - 1/2\epsilon_0\mathrm{E^2}(\chi_\mathrm{e} + \rho_\alpha(\delta\chi_\mathrm{e})(\delta\rho_\alpha)^{-1}) + \epsilon_0\chi_\mathrm{e}\mathrm{E_n^2}$, which is similar to the electric stress used in literature [20], but includes the effect of changes in the distribution of the electromagnetic dipoles in the drop due to the applied electric field.

To test the validity of Eq. (7), we experimentally investigate the shape of paramagnetic drops in a homogeneous magnetic field directed along the symmetry axis of the drop (Fig. 1). We use a C-frame adjustable electromagnet containing iron cores with tips of 8 mm diameter. The substrates are 1 mm thick microscope glass slides coated with superhydrophobic composite films from colloidal graphite [21]. To measure over a wide range of total magnetic moments ($\mathrm{J} = \chi\mathrm{VB}\mu_0^{-1}$), we apply fields of 0 to 0.6 T; use drop volumes of 40-100 μl; and use three different aqueous paramagnetic salt solutions: (1) 35.6% ppw ($\chi = 2.55 \times 10^{-5}$) and (2) 17.8% ppw ($\chi = 1.24 \times 10^{-5}$)

manganese chloride tetrahydrate ($MnCl_2 \cdot 4H_2O$) and (3) 51 % ppw ($\chi = 4.17 \times 10^{-5}$) gadolinium chloride hexahydrate ($GdCl_3 \cdot 6H_2O$) [22].

To analyse the shape of the drop, we developed an algorithm similar to the standard Axisymmetric Drop Shape Analysis [23]: by imaging the side-profile of the drop using a digital DSLR-camera and using computational image analysis, we determine the drop outline r(z); we solve Eq. (7) numerically for r(z), using the Runge-Kutta method; and iteratively fit the solution of Eq. (7) using a standard least-square method (Levenberg-Marquardt) to the left and right-side of the drop outline independently.

To obtain good fits of Eq. (7) to r(z) of (1) the drop in the absence of magnetic fields: we estimate the density of the solutions ρ to be equal to the density of water ($\rho_w = 997$ kgm^{-3}) and 1.1 times the density of water for the $MnCl_2$ and $GdCl_3$ solutions respectively and allow γ to freely change; and (2) the drop in the presence of magnetic fields: we allow $\xi_0\rho_\alpha$ to freely change. This numerical optimization of physical values allows us to account for errors in our estimates of (1) the surface tension and density of the drop; and (2) the value of the field-independent chemical potential and the value of the difference of the field-independent thermodynamic potentials of liquid and vapour phase ($a_0^l - a_0^v$). The uncertainty on the $a_0^l - a_0^v$ value is caused by a non-axisymmetric deformation of the drop, due to systematic errors such as inhomogeneties in the applied field and in the roughness of the substrate, and the coarseness of the manual levelling of the substrate and magnet. (Without a numerical optimization of $\xi_0\rho_\alpha$ (set to zero) we achieve less consistently good fits.) To measure the radius of curvature at the apex point, we fit a parabolic function to r(z) in the range where Eq. (7) vanishes. We measure the contact angles of the left and right side of the drop independently by fitting second-order polynomials to the outline of the drop close to the triple contact line.

An example result of this methodology is presented by Fig. 1. The side-profile photographs of a 60 μl drop of the aqueous 51.4% ppw $GdCl_3$ solution presented by Fig. 1(a) show a visible elongation of the drop along the field lines. The numerical solutions of Eq. (7) run smoothly along the outline as shown by Fig. 1(b), with the optimized numerical value γ =66.7 mNm^{-1}. The optimized surface tension is $\approx$ 8% smaller than that of water (72.8 mNm^{-1}), accounting errors in the initial guesses of the numerical values of density and surface tension. Over the range of investigated salt concentrations, the optimized surface tension values are (71.3±0.3(SE)) mNm^{-1}, (72.3±0.1(SE)) mNm^{-1}, and (69.8±0.5(SE)) mNm^{-1} for the 35.6% ppw $MnCl_2$, 17.8% ppw $MnCl_2$, and 51.4% ppw $GdCl_3$ solutions respectively and the field-independent chemical potential varies, independently of salt concentration, between

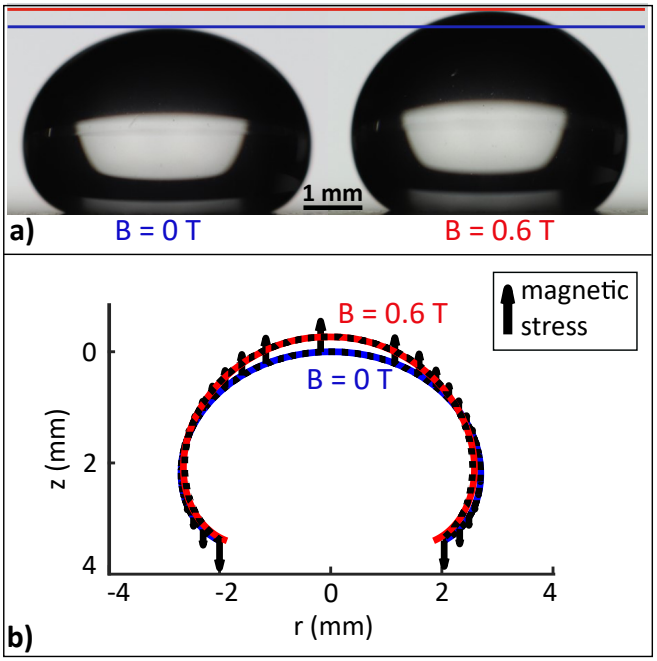

FIG. 1. **(a)** Images of a 60 μl drop of an aqueous solution with 51.4% ppw $GdCl_3$ in the absence and in the presence of a magnetic field. The drop is elongated along the direction of the field lines. **(b)** The outlines (black dashed) of the drop in (a), and the corresponding numerical solutions of Eq. (7) with a parabolic fit in the region around the apex point where the numerical solution collapses. The black arrows show the variation of the relative magnitude of the magnetic stress along the outline of the drop.

-(1.6±0.2(SE))×10^{-3} Jkg^{-1}.

Also presented by Fig. 1(b) is the magnetic stress acting on the outline of the drop. We observe that the stress is directed outwards from the drop along the magnetic field lines and its magnitude is proportional to the normal component of the magnetic flux density B_n^2. The magnetic stress is largest at the apex point, where the surface normal of the drop is parallel to the magnetic field lines, and diminishes at the outermost sides of the drop, before increasing again. At the solid-liquid interface, the surface vector of the drop is also parallel to the magnetic field lines, resulting in a magnetic stress and subsequent elongation of the drop towards the solid substrate which has not been studied here. This effect can be observed when suspending the droplet in a non-magnetizable medium [24]. Our investigation demonstrates the axisymmetric deformation of a paramagnetic drop through the application of a magnetic field that is axisymmetric with respect to the drop. A field that is not axisymmetric with respect to the drop, would cause a deformation towards the region of higher magnetic flux density.

Fig. 2 shows the change in characteristic geometric parameters of the drop presented by Fig. 1. As the

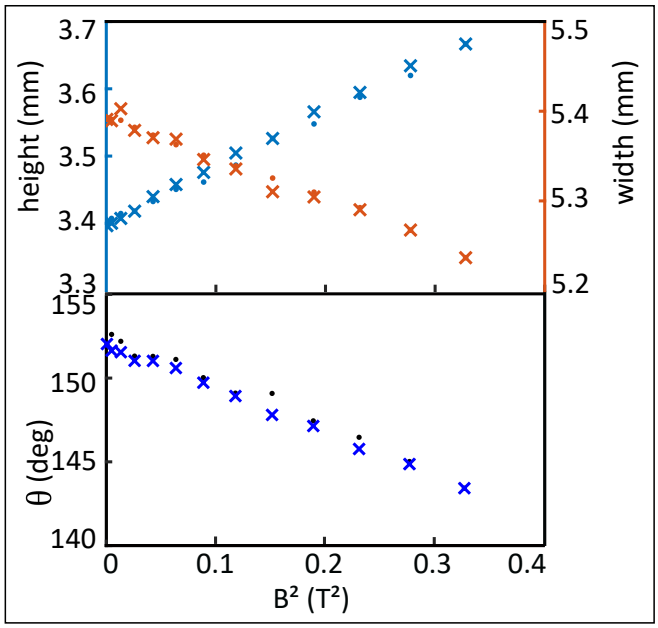

FIG. 2. Characteristic parameters of the shape of the drop presented by Fig. 1 as a function of the increasing (dots) and decreasing (x) applied field. (a) The height increases and the width decreases linearly with the square of the applied field. (b) The contact angle (θ) decreases linearly with the square of the applied field.

drop elongates along the field lines, the height increases from 3.4 to 3.7 mm, the width decreases from 5.39 to 5.24 mm, and the contact angle decreases from 152° to 143° between 0 T and 0.6 T applied field. The changes in height, width and contact angle are linear with B^2. The noise on the measurements originates from physical sources (vibrations induced in the drop from the laboratory environment), and from the grayscale to binary image conversion which introduces a random error caused by the background light and the pixel resolution of the camera. There is a small amount of hysteresis visible in the results shown by Fig. 2, which originates from the substrate properties (hysteresis in receding and advancing movement of the triple contact line). The deformation is fully reversible as long as the volume of the drop remains constant for the duration of the measurement.

Fig. 3 shows the change in height in the absence and presence of magnetic fields (B=0.5 T), of drops with a range of concentrations and volumes. The change in height increases with the drops total magnetic moment. Due to the linear relation between applied and induced field, the total magnetic moment of the drop increases proportionally with applied field. The proportionality constant between the total magnetic moment per unit volume and the applied field is the magnetic susceptibility. This result clearly illustrates the underlying electromagnetic theory presented in Eq. 1,

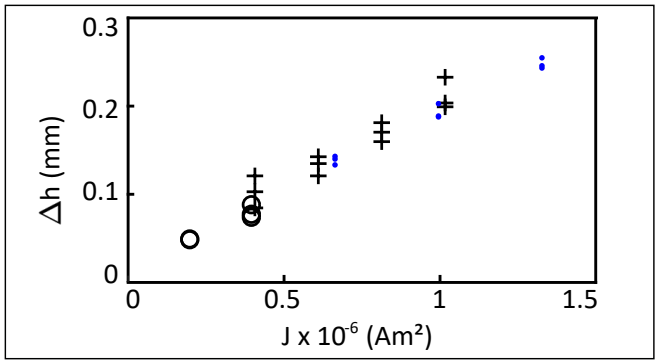

FIG. 3. The change in height (Δh) between 0 and 0.5 T applied field (B) of drops with different total magnetic moments (J). The change in height increases with total magnetic moment ($J=\chi VB\mu_0^{-1}$) of a drop with volume V and magnetic susceptibility χ. The three different markers represent the three salt solutions: 35.6% ppw $MnCl_2$ (crosses), 17.8% ppw $MnCl_2$ (circles), and 51.4% ppw $GdCl_3$ (dots) with $\chi = 2.55 \times 10^{-5}$, $\chi = 1.24 \times 10^{-5}$, and $\chi = 4.17 \times 10^{-5}$ respectively.

where the stress acting on the drop, and therefore the shape of the drop, is directly dependent on the exchange of momentum between matter and electromagnetic fields.

In conclusion, we have derived an expression for the shape of a magnetic drop in a magnetic field and validated this expression experimentally by analysing the shape of a paramagnetic drop in a homogeneous magnetic field. We have highlighted with this work that the fundamental symmetry of electric and magnetic phenomena in the electromagnetic stress tensor carries through to practical applications such as shape control of drops. This insight opens a whole range of applications to magnetic phenomena, such as display technologies, liquid lenses, and chemical mixing of drops in microfluidics.

This work was funded by the Centre for Doctoral Training in Integrative Sensing and Measurement: EP/L016753/1.

* corresponding author: adam.stokes@ed.ac.uk

[1] K. Mishra, D. van den Ende, and F. Mugele, Micromachines **7** (2016), 10.3390/mi7060102.
[2] M. J. Jebrail and A. R. Wheeler, Current Opinion in Chemical Biology **14**, 574 (2010).
[3] R. Seemann, M. Brinkmann, T. Pfohl, and S. Herminghaus, Reports on Progress in Physics **75**, 016601 (2011).
[4] E. Samiei, M. Tabrizian, and M. Hoorfar, Lab on a Chip **16**, 2376 (2016).
[5] G. Chen, B. Ji, Y. Gao, C. Wang, J. Wu, B. Zhou, and W. Wen, Sensors and Actuators, B: Chemical **286**, 181 (2019).
[6] K. Stierstadt and M. Liu, ZAMM Zeitschrift fur Angewandte Mathematik und Mechanik **95**, 4

[7] F. Mugele and J.-C. Baret, Journal of Physics: Condensed Matter **17**, R705 (2005).

[8] T. B. Jones, J. D. Fowler, Y. S. Chang, and C. J. Kim, Langmuir **19**, 7646 (2003).

[9] K. H. Kang, Langmuir **18**, 10318 (2002).

[10] G. McHale, C. V. Brown, M. I. Newton, G. G. Wells, and N. Sampara, Physical Review Letters **107**, 1 (2011).

[11] C. V. Brown, G. G. Wells, M. I. Newton, and G. McHale, Nature Photonics **3**, 403 (2009).

[12] H. Geng, J. Feng, L. M. Stabryla, and S. K. Cho, Lab on a Chip **17**, 1060 (2017).

[13] Y. Zhang and N.-T. Nguyen, Lab Chip **17**, 994 (2017).

[14] N. Pamme, Lab Chip **6**, 24 (2006).

[15] A. Egatz-Gómez, S. Melle, A. A. García, S. A. Lindsay, M. Márquez, P. Domínguez-García, M. A. Rubio, S. T. Picraux, J. L. Taraci, T. Clement, D. Yang, M. A. Hayes, and D. Gust, Applied Physics Letters **89** (2006), 10.1063/1.2227517.

[16] L. Mats, F. Logue, and R. D. Oleschuk, Analytical Chemistry **88**, 9486 (2016).

[17] C. A. Miller and P. Neogi, *Interfacial phenomena : equilibrium and dynamic effects*, 2nd ed., Surfactant science series ; v. 139 (CRC Press, London, 2008) pp. 1–29.

[18] V. A. Lubarda and K. A. Talke, Langmuir **27**, 10705 (2011).

[19] A. W. Adamson, *Physical chemistry of surfaces*, fifth edit ed. (New York : John Wiley & Sons, Inc., New York, 1990).

[20] L. T. Corson, C. Tsakonas, B. R. Duffy, N. J. Mottram, I. C. Sage, C. V. Brown, and S. K. Wilson, Physics of Fluids **26**, 122106 (2014).

[21] I. S. Bayer, V. Caramia, D. Fragouli, F. Spano, R. Cingolani, and A. Athanassiou, Journal of Materials Chemistry **22**, 2057 (2012).

[22] We calculate χ for the salt solution using: $\chi = (\chi_s^m C_s M_s^{-1} + \chi_w^m (1 - C_s) M_w^{-1})\rho$, where $M_s = 197.9 \times 10^{-3}$ kg mol^{-1} for $MnCl_2$, and $M_s = 371.7 \times 10^{-3}$ kg mol^{-1} for $GdCl_3$, and $M_w = 18.02 \times 10^{-3}$ kg mol^{-1} are the molecular masses, and $\chi_s^m = 14350 \times 10^{-12}$ m^{3}mol^{-1} for $MnCl_2$, and $\chi_s^m = 27930 \times 10^{-12}$ m^{3}mol^{-1} for $GdCl_3$, and $\chi_w^m = -12.63 \times 10^{-12}$ m^{3}mol^{-1} are the literature values for the molar magnetic susceptibilities of the paramagnetic salts and water respectively [25]. C_s and ρ are the weight concentration of the salt in the solution and the density of the solution respectively.

[23] S. M. Saad and A. W. Neumann, Advances in Colloid and Interface Science **238**, 62 (2016).

[24] S. Afkhami, A. J. Tyler, Y. Renardy, M. Renardy, T. G. St. Pierre, R. C. Woodward, and J. S. Riffle, Journal of Fluid Mechanics **663**, 358 (2010).

[25] J. R. Rumble, in *CRC Handbook of Chemistry and Physics, 99th Edition (Internet Version 2018)* (CRC Press/Taylor & Francis, Boca Raton, FL).